

Compact terahertz multiheterodyne spectroscopy using a Y-shape dual-comb configuration

Hua Li,^{*} Ziping Li, Kang Zhou, Xiaoyu Liao, Sijia Yang, and J. C. Cao

*Key Laboratory of Terahertz Solid State Technology,
Shanghai Institute of Microsystem and Information Technology,
Chinese Academy of Sciences, 865 Changning Road, Shanghai 200050, China and
Center of Materials Science and Optoelectronics Engineering,
University of Chinese Academy of Sciences, Beijing 100049, China*

Wenjian Wan and Chenjie Wang

*Key Laboratory of Terahertz Solid State Technology,
Shanghai Institute of Microsystem and Information Technology,
Chinese Academy of Sciences, 865 Changning Road, Shanghai 200050, China*

(Dated: April 10, 2019)

Abstract

Due to the fast and high resolution characteristics, the dual-comb spectroscopy attracts more and more interest since the first demonstration. In the terahertz frequency range where abundant absorption lines (finger-prints) of molecules are located, the multiheterodyne spectroscopy employing the dual-comb technique shows an advantage in real-time spectral detection over the traditional Fourier transform infrared or time domain spectroscopies. Here, we demonstrate the first compact terahertz multiheterodyne spectroscopy using a Y-shape dual-comb configuration without a need of additional fast detectors. With only ~ 270 nW terahertz power coupled into a terahertz QCL comb (no optics for alignment), the down-converted dual-comb spectra are successfully obtained at different carrier frequencies. To prove the spectroscopic ability, we further demonstrate that the compact dual-comb system can be used to calibrate the relative humidity in the air and to measure the transmission of a GaAs etalon. Due to the small optical coupling aperture (150 μm), it is also potential to use the dual-comb technique for terahertz imaging.

Compared to traditional Fourier transform infrared (FTIR) and time domain spectroscopies (TDS)¹⁻⁴, the dual-comb spectroscopy⁵⁻⁷ shows advantages not only in the fast data acquisition but also the high spectral resolution. In the terahertz frequency range, due to the high power and broad frequency coverage, the electrically-pumped terahertz quantum cascade laser (QCL)⁸ is an ideal candidate for dual-comb multiheterodyne spectroscopy.

Although the multiheterodyne detection using QCL combs have been already demonstrated using either a on-chip configuration^{9,10} or a laser + fast external detector system^{11,12}, a compact dual-comb system is still much in demand for practical applications. Concerning the on-chip dual comb, it is indeed compact, but it is impossible for substance detections because the whole system is in vacuum and no sample can be placed between the combs for spectral detections. Additionally, for the on-chip dual-comb configuration, the optical coupling between two laser combs is through the laser substrate. Therefore, even the on-chip dual-comb can work at room temperature in the open air, it is still problematic for substance detection. So the non-on-chip dual-comb is absolutely required for practical applications. For the multiheterodyne detection using fast terahertz detectors, i.e., Schottky mixers^{12,13}, superconducting hot-electron bolometer (HEB)^{12,14}, or quantum well infrared photodetectors¹⁵, it is feasible for detections of finger-prints of substances. However, the external fast detector will bring about complexities for the optical alignment and/or cooling.

In this work, we propose the most compact terahertz multiheterodyne spectroscopy based on a Y-shape dual-comb configuration. There is no moving part in the compact system and only one cryostat is needed. No optical mirror is used for the optical coupling and alignment. Multiple dual-comb spectra at different carrier frequencies resulted from free-space optical coupling are successfully obtained. Furthermore, the water absorption and transmission of a GaAs etalon are measured using the multiheterodyne spectroscopy. The microwave to terahertz frequency calibration is done with two water absorption lines.

Figure 1(a) shows the schematics of the compact terahertz dual-comb multiheterodyne spectroscopy. The two terahertz QCLs (Comb1 and Comb2) with a bound-to-continuum active region¹⁶ and single plasmon waveguides are placed face to face. One of the lasers, Comb2, is used as a fast detector for recording the down-converted dual-comb spectra. The QCL can be used as a fast detector because the fast inter-subband relaxation process in the active region¹⁷. Since the two laser combs are spatially separated, the multiheterodyne system can be used for fast spectral detection by putting samples between the laser combs. The compact multiheterodyne detection is made possible by delicately designing the Y-shape holder and the vacuum cap as shown in Fig.

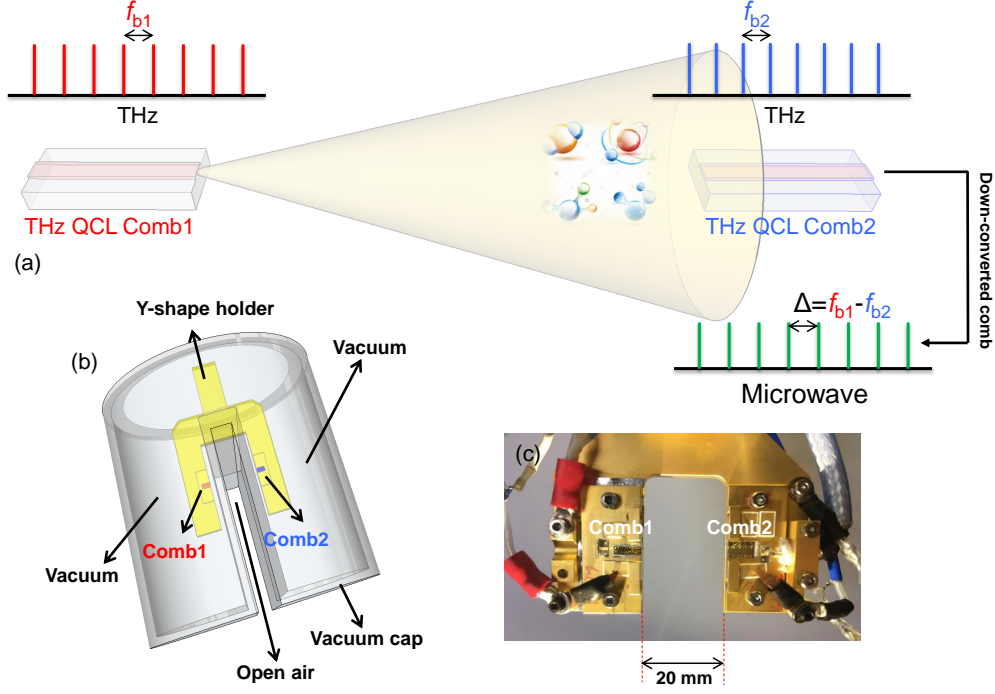


FIG. 1. Schematics of compact terahertz dual-comb multiheterodyne spectroscopy. (a) Optical coupling of the two terahertz QCL combs and illustration of microwave frequency synthesis. f_{b1} and f_{b2} denote the inter-mode beat note frequencies (or terahertz mode-spacings) of Comb1 and Comb2, respectively. (b) Transparent plot of the Y-shape dual-comb geometry. The two laser combs sit on the two branches of the Y-shape holder. The vacuum cap is delicately designed to retain the vacuum for both QCLs and simultaneously create an open air space (sample chamber) between the two laser combs. (c) Optical photo of the Y-shape holder. The distance between the two laser combs is 20 mm. The two lasers are based on a single plasmon waveguide and have identical dimensions (6 mm long cavity and 150 μm wide ridge).

1(b). The two laser combs sit on the two branches of the Y-shape holder and the vacuum cap made of high density polyethylene is designed to retain vacuum for both laser combs and simultaneously create a sample chamber [open air as shown in Fig. 1(b)] between the combs. Fig. 1(c) shows an optical photo of the Y-shape holder with the two laser combs mounted on the branches.

The multiheterodyne system shown in Fig. 1 is featured by its compactness without needs of additional fast detector and optics for alignment, which has been never reported before. From the schematic illustration shown in Fig. 1(a), we understand there is only a very small portion of the terahertz light from Comb1 coupled into Comb2. The power that is coupled into Comb2, P , can

be written as

$$P = P_0 \cdot \frac{S_{\text{eff}}}{S_0}, \quad (1)$$

where P_0 is the total power of Comb1 that reaches onto the entire plane of the facet of Comb2, S_0 is the beam area of Comb1 at the facet position of Comb2, and S_{eff} is the effective facet area of Comb2 that interacts with the light from Comb1. By considering a 50% loss (window transmission and water absorption), P_0 can be estimated to be 1.3 mW from the total measured power of 2.6 mW [see Fig. 2(a)]. $S_0 (\doteq 3.9 \times 10^{-5} \text{ m}^2)$ can be obtained by considering the far-field beam divergence of 20° [Fig. 2(b)] and the 20-mm distance between the two combs [see Fig. 1(c)]. Without optics for alignment, only very small portion of light can be coupled into Comb2. To evaluate the effect area (S_{eff}) of Comb2 that interacts with the light from Comb1, we perform the finite-element simulation for the QCL layer structure. In Fig. 2(c), we show the calculated two-dimensional electric field distribution at 4.2 THz. From the measured dimensions shown in Fig. 2(c), we can calculate the effective area $S_{\text{eff}} \doteq 8.09 \times 10^{-9} \text{ m}^2$. Finally, we are able to calculate the power that injects into Comb2 for the multiheterodyne process by following equation 1, i.e., $P = P_0 \cdot S_{\text{eff}} / S_0 \doteq 270 \text{ nW}$. Note that, similar as the on-chip dual-comb based on terahertz QCLs⁹, the strong optical coupling between the combs should be avoided due to the optical injection-locking effect.

Figure 3(a) schematically plots the different processes for generating dual-comb spectra at

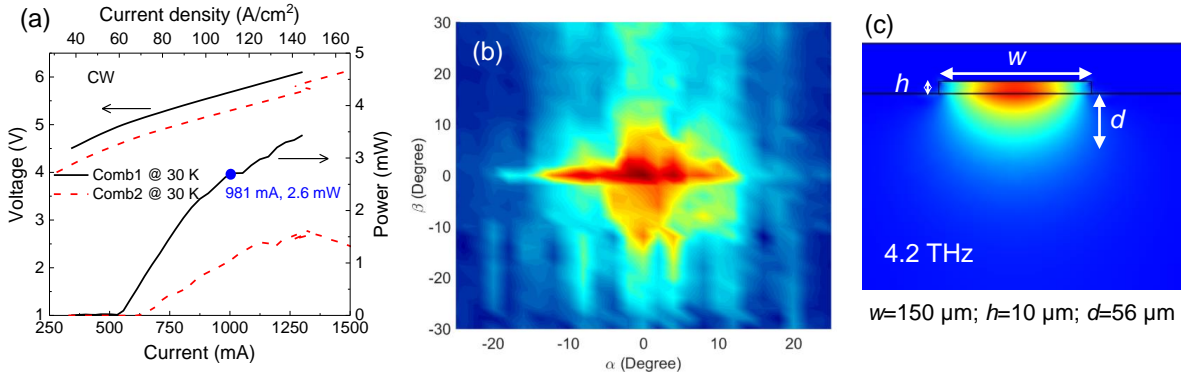


FIG. 2. (a) $L-I-V$ characteristics in continuous wave (CW) mode of the two lasers recorded at a stabilized temperature of 30 K. (b) Far-field beam profile of Comb1 measured in pulsed mode at a current of 1000 mA. (c) Calculated two-dimensional electric field distribution of the fundamental mode at 4.2 THz for the QCL structure used in this work. w , h , and d denote the ridge width, ridge height, and the depth into the substrate that the optical mode can reach, respectively.

different carrier frequencies in microwave range. All the four examples are resulted from beatings between one terahertz mode of Comb1 (red lines) and one terahertz mode of Comb2 (blue lines). It can be seen that not only the beating of neighbouring modes, but also beatings between modes that are far separated can generate dual-comb signals.

In Fig. 3(b), we show the inter-mode beat not signal measured by simultaneously switching on both lasers in continuous wave mode, i.e, 1000 and 945 mA for Comb1 and Comb2, respectively. Since the signal is measured via the microwave transmission line which is electrically connected to Comb2, the signal at f_{b2} is much stronger than f_{b1} . The frequency difference between f_{b1} and f_{b2} is measured to be 8 MHz which determines the line spacing of the down-converted dual-comb

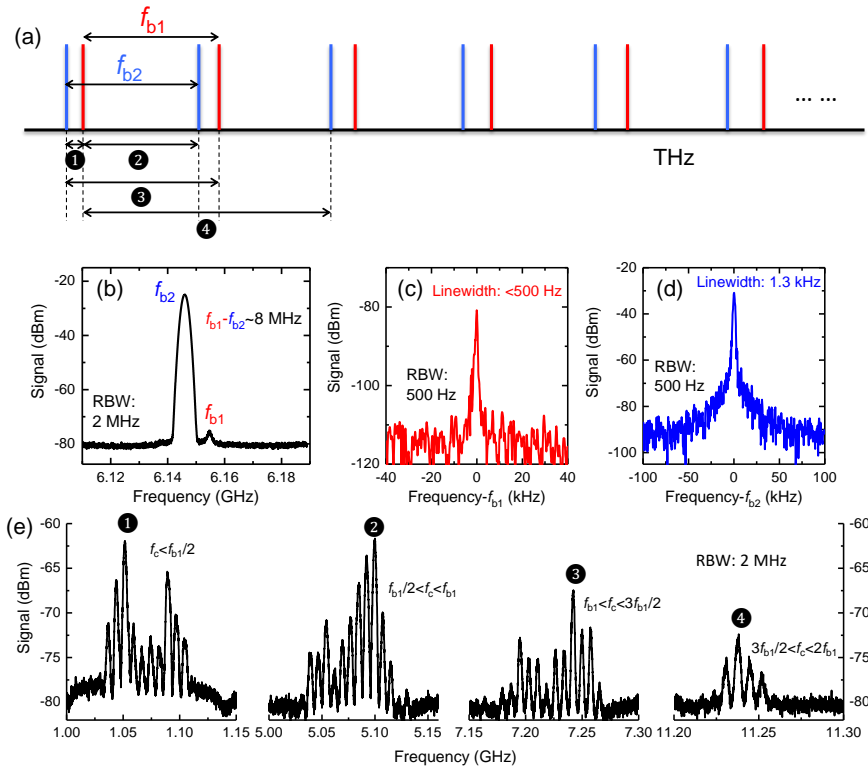


FIG. 3. Dual-comb generations at multiple carrier frequencies. (a) Schematic of dual-comb generation processes. f_{b1} and f_{b2} are the inter-mode beat note frequencies of Comb1 and Comb2, respectively. ①, ②, ③, and ④ represent different beating processes for generating dual-comb spectra at different carrier frequencies. (b) Inter-mode beat notes measured from Comb2 with a RBW of 2 MHz. The frequency difference between f_{b1} and f_{b2} is 8 MHz. (c) and (d) are the measured linewidths of f_{b1} and f_{b2} , respectively. (e) Measured dual-comb spectra at different carrier frequencies. QCL Comb1 and Comb2 are operated at 1000 and 945 mA, respectively, in cw. The heat sink temperature is stabilized at 20 K.

spectra shown in Fig. 3(e). The high resolution spectra for Comb1 and Comb2 are shown in Figs. 3(c) and 3(d), respectively, measured using a resolution bandwidth (RBW) of 500 Hz. It is shown that although the signal of Comb1 is much weaker, its frequency stability is much better than Comb2. The linewidths of f_{b1} and f_{b2} are measured to be <500 Hz and 1.3 kHz, respectively.

The measured down-converted dual-comb spectra at different microwave frequencies following the processes ①, ②, ③, and ④ are shown in Fig. 3(e). The line numbers of the spectra recorded at different carrier frequencies are not the same, which is due to the differences in nonlinear mixing strengths of terahertz modes and signal attenuations of microwave cables at different frequencies. However, the spectra shown in Fig. 3(e) sufficiently prove that the dual-comb multiheterodyne beating is successfully obtained in the compact system shown in Fig. 1.

To further demonstrate the free-space optical coupling and real-time detection characteristics of the multiheterodyne dual-comb system, we recorded a film to show that the dual-comb spectra with an A4 paper or metal board blocked in the beam path can be obtained in real time (see Visualization 1).

In Fig. 4, we verify that the multiheterodyne system is capable of spectroscopic applications. Figure 4(a) shows the terahertz emission spectra of Comb1 and Comb2 driven at 981 and 1015 mA, respectively, at a stabilized heat sink temperature of 34.5 K. The shaded area sketches the frequency range where the two combs strongly interact with each other for generating dual-comb spectra [see inset of Fig. 4(b)]. The first spectroscopy is performed with the sample of water vapor. We change the relative humidity (RH) of the sample chamber and measure dual-comb spectra with an optical bandwidth of 120 GHz at the frequency around 5 GHz as shown in the inset of Fig. 4(b). Then, the peaks are taken from the dual-comb spectra for all 21 lines at different RH values. The main results are plotted in Fig. 4(b) for RH values between 1% to 80%. We can see that the intensities of modes 6 and 10 in dual-comb spectra decrease with increasing RH. The two lines (modes 6 and 10) correspond to the two strong water absorption lines at 4.17 and 4.19 THz which are shown as the gray lines in Fig. 4(b) extracted from HITRAN database. It is worth noting that the two water lines can be used to calibrate the microwave frequency of the measured dual-comb spectrum to terahertz frequency regime. The calibrated terahertz frequencies for dual-comb lines from mode 1 to 21 are between 4.139 to 4.261 THz, covering a frequency bandwidth of 122 GHz which agrees well with the frequency range shown in Fig. 4(a) for generating dual-comb spectra.

To further investigate the RH-dependence of the dual-comb spectra, in Fig. 4(c) the intensity of modes 6 (red) and 10 (green) is plotted as a function of RH. It can be clearly seen that as RH

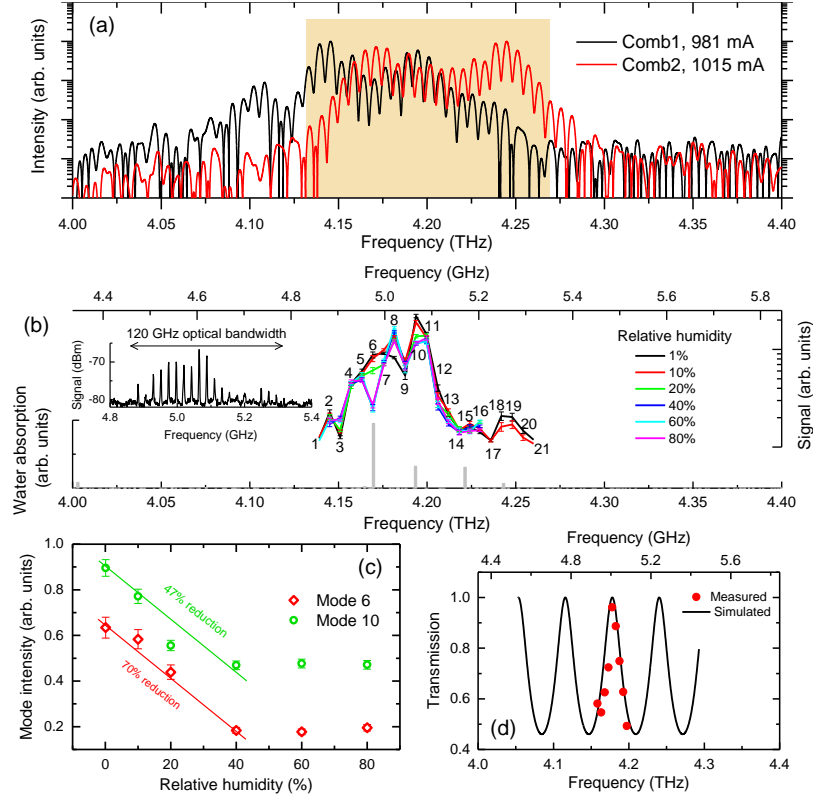


FIG. 4. Terahertz dual-comb multiheterodyne spectroscopy. (a) Emission spectra of the QCL Comb1 (black) and Comb2 (red) measured using a FTIR spectrometer. The shaded area depicts the frequency regime where the two laser combs are spectrally overlapped for dual-comb generations. (b) Peak intensities of dual-comb spectra at different relative humidity values. The numbers from 1 to 21 denote the mode index of the dual-comb spectra. The water absorption lines obtained from the HITRAN database are also shown in (b) for frequency calibration from microwave to terahertz frequencies. The inset shows a typical dual-comb spectrum measured with a relative humidity value of 1%. (c) Mode intensity as a function of relative humidity for two water lines (mode 6 and 10). The scatters are measured results and solid lines show the linear relationship between mode intensity and relative humidity of being from 1% to 40%. (d) Transmission of a 625- μm -thick GaAs etalon measured using the terahertz dual-comb spectroscopy. Circles are the extracted peak intensities from the dual-comb lines. The black curve is a simulation for comparison. All the data were recorded when Comb1 and Comb2 were operated at 981 and 1015 mA, respectively, in cw at a stabilized heat sink temperature of 34.5 K. Each dual-comb spectrum was measured for 6 times and a deviation for each dual-comb lines was then obtained, which gives the amplitude noises or error bars of all dual-comb lines.

increases from 1% to 40%, the mode intensity shows a good linear dependence with RH for both modes 6 and 10. However, when RH is beyond 40%, no visible change with RH can be observed for both modes, which is a sign of the absorption saturation. Due to the linear dependence between 1% and 40% RH, this dual-comb technique can be used to measure the RH value in real time. Since the two modes show different intensity-RH dependences, the accurate measurement can be done with calibrations with each other.

We also employ the dual-comb multiheterodyne system to measure the transmission of a GaAs etalon to further verify its ability for spectroscopy. Figure 4(d) shows the measured transmission of a 625- μm -thick GaAs etalon (red circles) together with the simulated transmission (black curve). Same as before, the frequency calibration from microwave to terahertz frequency is done with the two absorption lines shown in Fig. 4(b). The experimental data shown in Fig. 4(d) are obtained by ratioing the peak intensities of the dual-comb spectra measured with and without the GaAs etalon. The simulation is performed by employing a transfer matrix method¹⁸. Unfortunately, due to the thick sample, the effective optical bandwidth for this measurement is only 50 GHz from 4.15 to 4.20 THz. The agreement between the experimental data and simulation verifies that the multiheterodyne system is capable of real time spectroscopies and fast substance identifications.

Although the real-time terahertz spectroscopy system employing the dual-comb technique is successfully demonstrated, there are still some work to do in the future to optimize the system. First of all, in current work, the two lasers are operated in free running. The frequency stability and the optical bandwidth, in principle, can be significantly improved by external radio frequency (RF) injections^{17,19,20}. By doing so, the down-converted dual-comb spectrum can be widened to cover more finger prints of substances, and therefore, the compact multiheterodyne system can then be used for broader applications. The RF injection can also fine tune the terahertz frequency for high resolution spectroscopy. Secondly, to improve the signal to noise ratio of the multiheterodyne lines, the distance between the two laser combs which determines the coupling strength of the two combs should be optimized to find a balance between the optical coupling and injection locking. Thirdly, the relative phase relationship between the two sets of modes could be further locked to increase the system stability. This can be achieved by sending one of the dual-comb lines to a phase lock loop module and then lock all the multiheterodyne lines without locking the carriers of the combs.

It has to mention that besides the spectroscopic application, the compact multiheterodyne system can be also used for terahertz imaging. Different from the imaging using the terahertz intensity

signal^{21–23}, inter-mode beat note^{24,25}, or self-mixing^{26,27}, the multiheterodyne imaging can also provide spectral information as well as the imaging information (transmission or reflection). Note that, as we already elaborated previously, the effective area (S_{eff}) for the dual-comb multiheterodyne detection is roughly determined by the laser ridge size. Therefore, the spatial resolution of the dual-comb multiheterodyne imaging is around 150 μm which is equivalent to that of a traditional terahertz imager. Furthermore, due to the nature of fast detection and mature techniques for microwave signal processing, the multiheterodyne imaging shows a potential advantages in fast signal detection and post-processing over the traditional terahertz intensity imaging.

In summary, we have demonstrated the most compact terahertz multiheterodyne spectroscopy employing a Y-shape laser-based dual-comb configuration. Without moving parts, optics mirrors, or fast detectors, the real-time (millisecond acquisition time) multiheterodyne spectroscopy has been successfully achieved with only 270 nW terahertz light coupled into the laser comb. The multiheterodyne system with an optical bandwidth of 120 GHz (21 modes) shows the spectroscopic abilities for fast water absorption and etalon transmission measurements. Due to its compactness, the portable system can be practically implemented in various application scenes for fast spectroscopy and/or toxic substance identifications. It also finds potential applications in the fast terahertz imaging.

This work is supported by the "Hundred-Talent" Program of Chinese Academy of Sciences, the National Natural Science Foundation of China (61875220, 61575214, 61404150, 61405233, and 61704181), the National Key R&D Program of China (2017YFF0106302), and Shanghai Municipal Commission of Science and Technology (17YF1430000).

* hua.li@mail.sim.ac.cn

¹ M. M. Coleman and P. C. Painter, *Applied Spectroscopy Reviews* **20**, 255 (1984).

² M. Vanexter, C. Fattering, and D. Grischkowsky, *Optics Letters* **14**, 1128 (1989).

³ I. C. Ho, X. Y. Guo, and X. C. Zhang, *Optics Express* **18**, 2872 (2010).

⁴ P. Y. Han, M. Tani, M. Usami, S. Kono, R. Kersting, and X. C. Zhang, *Journal of Applied Physics* **89**, 2357 (2001).

⁵ T. Udem, R. Holzwarth, and T. W. Hänsch, *Nature* **416**, 233 (2002).

⁶ B. Bernhardt, A. Ozawa, P. Jacquet, M. Jacquy, Y. Kobayashi, T. Udem, R. Holzwarth, G. Guelachvili,

- T. W. Hänsch, and N. Picque, [Nature Photonics 4, 55 \(2010\)](#).
- ⁷ I. Coddington, N. Newbury, and W. Swann, [Optica 3, 414 \(2016\)](#).
- ⁸ R. Köhler, A. Tredicucci, F. Beltram, H. E. Beere, E. H. Linfield, A. G. Davies, D. A. Ritchie, R. C. Iotti, and F. Rossi, [Nature 417, 156 \(2002\)](#).
- ⁹ M. Rösch, G. Scalari, G. Villares, L. Bosco, M. Beck, and J. Faist, [Applied Physics Letters 108, 171104 \(2016\)](#).
- ¹⁰ M. Rösch, M. Beck, M. J. Suess, D. Bachmann, K. Unterrainer, J. Faist, and G. Scalari, [Nanophotonics 7, 237 \(2018\)](#).
- ¹¹ G. Villares, A. Hugi, S. Blaser, and J. Faist, [Nature Communications 5, 5192 \(2014\)](#).
- ¹² Y. Yang, D. Burghoff, D. J. Hayton, J. R. Gao, J. L. Reno, and Q. Hu, [Optica 3, 499 \(2016\)](#).
- ¹³ A. Danylov, N. Erickson, A. Light, and J. Waldman, [Optics Letters 40, 5090 \(2015\)](#).
- ¹⁴ H. Richter, A. D. Semenov, S. G. Pavlov, L. Mahler, A. Tredicucci, H. E. Beere, D. A. Ritchie, K. S. Il'in, M. Siegel, and H. W. Hubers, [Applied Physics Letters 93, \(2008\)](#).
- ¹⁵ H. Li, W.-J. Wan, Z.-Y. Tan, Z.-L. Fu, H.-X. Wang, T. Zhou, Z.-P. Li, C. Wang, X.-G. Guo, and J.-C. Cao, [Scientific Reports 7, 3452 \(2017\)](#).
- ¹⁶ M. Wienold, L. Schrottke, M. Giehler, R. Hey, W. Anders, and H. T. Grahn, [Applied Physics Letters 97, 071113 \(2010\)](#).
- ¹⁷ H. Li, P. Laffaille, D. Gacemi, M. Apfel, C. Sirtori, J. Leonardon, G. Santarelli, M. Rösch, G. Scalari, M. Beck, J. Faist, W. Hänsel, R. Holzwarth, and S. Barbieri, [Optics Express 23, 33270 \(2015\)](#).
- ¹⁸ H. Li, J. M. Manceau, A. Andronico, V. Jagtap, C. Sirtori, L. H. Li, E. H. Linfield, A. G. Davies, and S. Barbieri, [Applied Physics Letters 104, 241102 \(2014\)](#).
- ¹⁹ P. Gellie, S. Barbieri, J. F. Lampin, P. Filloux, C. Manquest, C. Sirtori, I. Sagnes, S. P. Khanna, E. H. Linfield, A. G. Davies, H. Beere, and D. Ritchie, [Optics Express 18, 20799 \(2010\)](#).
- ²⁰ S. Barbieri, M. Ravaro, P. Gellie, G. Santarelli, C. Manquest, C. Sirtori, S. P. Khanna, E. H. Linfield, and A. G. Davies, [Nature Photonics 5, 306 \(2011\)](#).
- ²¹ J. Darmo, V. Tamosiunas, G. Fasching, J. Kroll, K. Unterrainer, M. Beck, M. Giovannini, J. Faist, C. Kremser, and P. Debbage, [Optics Express 12, 1879 \(2004\)](#).
- ²² A. W. M. Lee, Q. Qin, S. Kumar, B. S. Williams, and Q. Hu, [Applied Physics Letters 89, 141125 \(2006\)](#).
- ²³ Z. Zhou, T. Zhou, S. Zhang, Z. Shi, Y. Chen, W. Wan, X. Li, X. Chen, N. Gilbert Corder Stephanie, Z. Fu, L. Chen, Y. Mao, J. Cao, G. Omenetto Fiorenzo, M. Liu, H. Li, and H. Tao Tiger, [Advanced Science 5, 1700982 \(2018\)](#).

- ²⁴ S. Barbieri, J. Alton, C. Baker, T. Lo, H. E. Beere, and D. Ritchie, [Optics Express](#) **13**, 6497 (2005).
- ²⁵ T. Zhou, H. Li, W. J. Wan, Z. L. Fu, and J. C. Cao, [AIP Advances](#) **7**, 105215 (2017).
- ²⁶ P. Dean, Y. L. Lim, A. Valavanis, R. Kliese, M. Nikolic, S. P. Khanna, M. Lachab, D. Indjin, Z. Ikonc, P. Harrison, A. D. Rakic, E. H. Linfield, and A. G. Davies, [Optics Letters](#) **36**, 2587 (2011).
- ²⁷ M. Wienold, T. Hagelschuer, N. Rothbart, L. Schrottke, K. Biermann, H. T. Grahn, and H. W. Hubers, [Applied Physics Letters](#) **109**, 011102 (2016).